Available online at www.sciencedirect.com
ScienceDirect
Trans. Nonferrous Met. Soc. China 29(2019) 876−892
Transactions of Nonferrous Metals Society of China
www.tnmsc.cn

Synthesis, in-situ coating and characterization of scorodite with high leaching stability

Ping-chao KE, Zhi-hong LIU

School of Metallurgy and Environment, Central South University, Changsha 410083, China

Received 10 April 2018; accepted 24 October 2018

Abstract: To improve stability of scorodite, a method of simultaneous synthesis and in-situ coating of scorodite was proposed. Scorodite particles with polyhedral and raspberry-like morphologies were synthesized in an Fe(II)−As(V)−H_2O system at 90 °C and pH 1.5 by blowing oxygen gas into the system. When the initial Fe/As molar ratio exceeded 1:1, a coating of sulfate-containing iron (hydr)oxides formed on the surfaces of scorodite particles during synthesis. To evaluate the leaching stability of synthesized scorodite samples, toxicity characteristic leaching procedure (TCLP) tests were conducted at pH 4.93 for 60 h, and long-term leaching tests were conducted for 30−40 d within a pH range of 5.40−10.88. The leaching results indicated that the release of arsenic from scorodite was noticeably postponed by the coating, and the average arsenic concentrations in the leaching solutions were as low as 0.12 mg/L in the TCLP tests and lower than 0.5 mg/L in the long-term leaching tests.
Key words: scorodite; arsenic immobilization; nucleation; in-situ coating; stability

1 Introduction

Arsenic is toxic to most living creatures on the planet [1,2]. During the past two decades, arsenic use has been declining due to its high toxicity and carcinogenicity. Arsenic is, therefore, a "surplus element," meaning that its yield is higher than its consumption [3]. Arsenic is widely associated with the ores or concentrates of nonferrous metals [4], especially copper, gold, and lead−zinc ores [5]. During nonferrous metallurgy, arsenic is enriched in arsenic-bearing materials such as flue dust, residues, anode slimes, and black copper sludge. To solve the problem of arsenic accumulation in the production system, and to protect the environment from arsenic pollution, arsenic should be removed from these materials, and then immobilized and safely collected in a specially managed field [6−8]. Therefore, the precipitation of arsenic from arsenic-bearing solutions into a stable mineral, a process known as "arsenic immobilization in a mineral," has been a challenging topic that has received great interest [9].

The main methods that are currently applied for bulk arsenic removal and disposal from arsenic-bearing solutions can be summarized as follows: neutralization with lime, precipitation as arsenic sulfide, neutralization with lime plus ferric iron, and immobilization as scorodite [10]. A series of calcium arsenate compounds, such as haidingerite, pharmacolite, guerinite and weilite, can precipitate from the Ca(II)−As(V)−H_2O system during lime neutralization [11]. However, these compounds are unstable in an acidic medium; furthermore, they will react with carbon dioxide in the air to produce calcium carbonate during stockpiling, releasing arsenic back into the environment [12,13]. Arsenic sulfide is prone to atmospheric and bacterial oxidation, and cannot be stably stockpiled [14]. Neutralization with lime plus ferric iron is an effective method for treating dilute arsenic-bearing solutions. During this process, a solution containing ferric and arsenate ions is neutralized by lime to produce ferrihydrite, a ferric oxyhydroxide phase, and gypsum [15], while arsenic is immobilized as arsenical ferrihydrite [16] because ferrihydrite has strong arsenic absorptivity. The precipitation of arsenical ferrihydrite is favored within a pH range of 4−7 [17]. In the presence of cations such as Zn(II), Cd(II), Pb(II), Ca(II) and Mg(II), a portion of the arsenic precipitates as Me-arsenates at a pH higher than 10 [16]. Furthermore, an amorphous or poorly crystalline ferric arsenate begins to precipitate

Foundation item: Project (51574285) supported by the National Natural Science Foundation of China
Corresponding author: Zhi-hong LIU; Tel: +86-13873117863; E-mail: zhliu@csu.edu.cn
DOI: 10.1016/S1003-6326(19)64998-8

within an approximate pH range of 1−5 and Fe/As molar ratio of 3−5 during this process [18]. This process can reduce arsenic concentration to 0.1 mg/L [19], but it consumes large amounts of lime and iron salt, and produces a high volume of residues.

Scorodite ($FeAsO_4·2H_2O$) has been recognized as a promising mineral for arsenic immobilization due to its good stability, low operation cost, high arsenic content (32.47 wt.%) and good crystallinity, which favors liquid to solid separation [20−23]. Scorodite can precipitate from acidic solutions that contain arsenic and iron under both hydrothermal and atmospheric conditions. The atmospheric process is more promising due to its low operation cost [24,25].

DEMOPOULOS et al [26,27], McGill University, Canada, were the first to develop a method for synthesizing scorodite under atmospheric conditions. The process was conducted in an Fe(III)−As(V)−H_2O system at approximately 90 °C. FUJITA et al [10], Dowa Metals & Mining Co., Ltd., Japan, developed another atmospheric method of scorodite synthesis, which was conducted in an Fe(II)−As(V)−H_2O system with an initial pH of 1.2−1.5. The scorodite particles precipitated during this process are large with a polyhedral morphology and show good stability under toxicity characteristic leaching procedure (TCLP) testing. Another advantage of this process is that it can be fulfilled within 7 h [28].

Scorodite is only stable under weakly acidic (pH 2.0−6.0) and oxidative conditions, and will release a large amount of arsenic if the pH is less than 2.0 or larger than 6.0, or under reductive conditions [29,30]. Therefore, to safely stockpile scorodite under various geographic and climatic conditions, its stability should be increased. Encapsulation of scorodite may be an effective method of improving its stability; many studies have been published in this field, for example, some have explored coating using silicate, phosphate or aluminum hydroxyl gels [31−33]. The results of these studies indicated that aluminum phosphate and aluminum hydroxyl appeared effectively at controlling the release of arsenic; however, sodium silicate gel strengthened the release of arsenic due to the ion exchange between SiO_4^{2-} and AsO_4^{3-}.

This paper reported a scorodite synthesis process, as well as the characteristics of the scorodite synthesized by the process. The process was an improvement method of FUJITA et al [10], and included two aspects. Firstly, the feeding of the ferrous sulfate solution was changed from rapid mixing to continuous addition within a certain time period; secondly, the pH of the slurry was maintained at 1.50 by inputting a sodium carbonate solution to neutralize the acid released throughout the synthesis process. It was found that, when the initial Fe/As molar ratio in the synthesis exceeded 1:1, an amorphous iron (hydr)oxide coating could form in-situ on the surfaces of the synthesized scorodite particles, which significantly improved their stability.

2 Experimental

2.1 Synthesis of scorodite

2.1.1 Materials

All chemicals used in this study, i.e. arsenic trioxide (As_2O_3), hydrogen peroxide (H_2O_2, 30%), ferrous sulfate heptahydrate ($FeSO_4·7H_2O$), and sodium carbonate (Na_2CO_3), were analytically pure and purchased from Sinopharm Chemical Reagent Co., Ltd., Shanghai, China. Compressed oxygen gas (99.9% purity, Saizhong Gas Co., Ltd., Changsha, China) was used as an oxidizing agent.

2.1.2 Synthesis apparatus

A diagram of the experimental apparatus for synthesis is presented in Fig. 1. The starting solution was placed in a 1 L cylindrical quartz glass reactor and heated by a thermostatic water bath with a temperature fluctuation of ±1 °C. Two thermometers with a 200 °C-measuring range were separately immersed into the reactor and water bath for measuring the synthesis temperature precisely. $FeSO_4$ and Na_2CO_3 solutions were added dropwise into an H_3AsO_4 solution by two low-speed constant-flow pumps. The slurry was stirred with a stainless-steel impeller coated by PTFE (polytetrafluoroethylene). The impeller was driven by a motor. Oxygen gas, with a flow rate controlled by a flowmeter, was scattered into the slurry through a bubble stone with a diameter of 8 cm, which was added to the bottom of the reactor. A condenser pipe was set into the top of the reactor to prevent slurry evaporation.

2.1.3 Preparation of solutions

In the nonferrous metallurgy process, the arsenic concentration in the leaching solution of high-arsenic materials is within an approximate range of 10−30 g/L [34]. According to the investigation conducted by FUJITA et al [10], the appropriate concentration of arsenic for larger, polyhedral scorodite particle formation was within a range of 30−50 g/L. Therefore, in this study, a 30 g/L arsenate solution was prepared using As_2O_3 as the arsenic source and hydrogen peroxide as the agent to oxidize As(III) into As(V). Hydrogen peroxide is an effective agent for oxidizing As(III), which had been demonstrated by many researchers [34,35]. According to the investigation conducted by CAETANO et al [36], As(III) was completely oxidized by hydrogen peroxide within 1 h with 20% stoichiometric excess.

The arsenate solution (30 g/L As) was prepared via following procedures. Firstly, 100 g of As_2O_3, 2 L of deionized water, and 400 g of 30% H_2O_2 (approximately

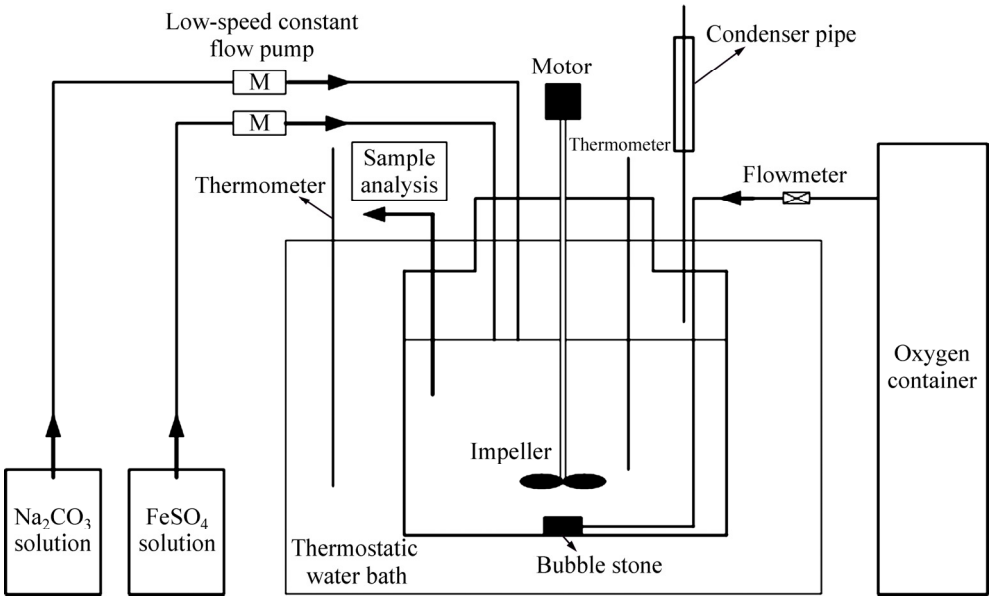

Fig. 1 Experimental apparatus of scorodite synthesis

250% stoichiometric excess) were mixed into a slurry in a 3 L closed reactor. The reactor was then heated in a water bath at (100±1) °C for 12 h, and the slurry was stirred continuously at 150 r/min by an impeller. During the first 1 h of heating, the solid As_2O_3 in the slurry dissolved completely; during the remaining 11 h of heating and reactions, the oxidation of As(III), together with the decomposition of excess H_2O_2 into O_2 and H_2O, was completed. Finally, the arsenic concentration in the prepared arsenate solution was calibrated to 30 g/L with the addition of deionized water. During the oxidation process of As(III), the oxidation rate was monitored after the As_2O_3 solids dissolved completely by sampling and analyzing at different time intervals and the results are shown in Fig. 2. It can be seen that about 75% As(III) has been oxidized in the period of As_2O_3 dissolution, and then the remaining As(III) was oxidized completely in 20 min after the dissolution. The valence states and

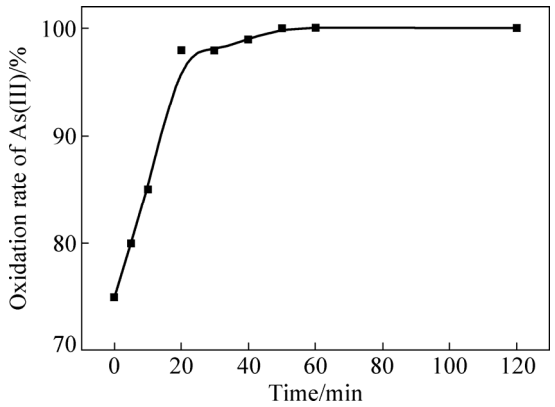

Fig. 2 Oxidation rate of As(III) as function of time at (100±1) °C

concentrations of arsenic were analyzed by inductively coupled plasma mass spectroscopy (ICP−MS, Thermo scientific/XSERIES 2).

To maintain the slurry volume during synthesis, $FeSO_4$ solutions were prepared with different concentrations according to initial Fe/As molar ratios of 1:1, 2:1, and 3:1, and the pH of the $FeSO_4$ solution was adjusted to 1.5±0.05 by the dropwise addition of a H_2SO_4 solution. A 1 mol/L Na_2CO_3 solution was prepared and used as a neutralizing agent.

2.1.4 Synthesis process

A 250 mL arsenate solution (30 g/L As), the pH of which was adjusted to 1.50±0.05 by the dropwise addition of a NaOH solution (0.8 mol/L), was added to a 1 L quartz glass cylindrical reactor. Then, based on the initial Fe/As molar ratios mentioned above, 250 mL of $FeSO_4$ solution with different concentrations was added to the reactor by a low-speed constant flow pump at a rate of (4.17±0.01) mL/min for 1 h. During $FeSO_4$ solution feeding, another low-speed constant flow pump was used to add a Na_2CO_3 solution (1 mol/L) into the reactor to maintain the pH of the slurry at 1.5±0.05. The volumes of Na_2CO_3 solution (1 mol/L) added were 42.0, 35.2, and 26.7 mL, corresponding to initial Fe(II)/As(V) molar ratios of 1:1, 2:1, 3:1, respectively. Afterwards, the slurry continued to be heated and stirred for 6 h. During the synthesis process, pure oxygen flowed continuously into the slurry at a rate of 1 L/min, and the temperature and stirring speed were maintained at (90±1) °C and 250 r/min, respectively. When synthesis had completed, the slurry was filtered through a 0.4 μm pore PTFE membrane and washed with 100 mL of acidified deionized water (pH 2.0) prepared with nitric acid

solution three times. It was then dried at (60±1) °C for 24 h. The dried samples were pulverized in a mortar to prepare them for the characterization and leaching tests.

In this study, three samples, denoted as S1, S2, and S3, were synthesized at initial Fe/As molar ratios of 1:1, 2:1 and 3:1, respectively.

A sodium carbonate solution was selected as the neutralizing agent during synthesis based on the following reasoning. Scorodite was precipitated during the synthesis process according to Eq. (1):

$$H_3AsO_4+Fe^{2+}+1/4O_2+3/2H_2O=FeAsO_4\cdot 2H_2O+2H^+ \quad (1)$$

Therefore, protons were continually released into the system with the precipitation of scorodite, thus, the pH of the system during synthesis decreased to approximately 0 after 1 h and was then maintained during the remaining 6 h without neutralization. As FUJITA et al [10] reported, the optimal pH for scorodite synthesis ranged from 1.5 to 2.0. It has been reported that the precipitation of Fe(III) through hydrolysis began at pH 1.5 [37]. Therefore, a neutralizing agent should be used to maintain the pH at 1.5 during synthesis. We conducted several experiments to choose an appropriate neutralizing agent. Agents such as sodium hydroxide, potassium hydroxide, sodium bicarbonate, and calcium oxide were investigated, and the results showed that these agents were insufficient as they had some shortcomings. Sodium hydroxide, potassium hydroxide, and sodium bicarbonate led to rapid Fe(III) hydrolysis, forming a large amount of ferric (hydr)oxide colloids that affected the formation of scorodite, thereby producing a precipitate with no scorodite; calcium oxide produced a precipitate with a large amount of gypsum, which would interfere the characterization of scorodite. Sodium carbonate was selected as the neutralizing agent in our experiments as it was the most suitable.

2.2 Analysis and characterization

2.2.1 Solutions

The total arsenic, iron, and sulfur concentrations in the solutions were measured by ICP−AES during routine analyses (Thermo scientific/iCAP 7000 SERIES, RF power 1150 W; auxiliary gas 0.50 L/min; analysis pump rate 1000 r/min). The As(III) concentrations in the solutions were also analyzed by ICP−AES. During As(III) analysis, to reduce As(III) to AsH_3 gas, a 1 mol/L KHB_4 solution was introduced into the flame launcher during sample injection. The intensity of the AsH_3 spectrum was characterized to determine the As(III) concentration. Before testing the samples, a standard curve was obtained from As(III) standard solutions, which were pre-reduced for 24 h by thiourea (0.2 g thiourea and 10 mL As(III)) to eliminate the small amount of As(V) that could have been present. The method was then calibrated by a standard, 0.1 mg/L As(III) solution (purchased from Central Iron & Steel Research Institute, Beijing, China). The As(III) detection limit of the instrument was 0.01 mg/L.

2.2.2 Solid samples

For the solid samples, X-ray diffraction (XRD) measurements were taken on a Rigaku RINT−200 instrument (Cu K_α), and the diffraction patterns in a 2θ range from 10° to 80° were obtained at a scanning rate of 1 (°)/s. Scanning electron microscopy (SEM) observation was conducted using a JEOL SM−6360LV. Transmission electron microscopy (TEM), high resolution transmission electron microscopy (HRTEM), and transmission electron microscopy with energy dispersive X-ray technical (TEM/EDX) observations were conducted using a Thermo Fisher TECNAI G2 F20; high resolution, high-angle annular dark field images (HAADF; ∼0.08 nm) and energy dispersive X-ray spectrometry (EDS) spectra were obtained using an FEI-Titan G^2 60−300 operated at 300 kV in the STEM mode. The samples were dispersed with ethyl alcohol at a liquid/solid mass ratio (L/S) of 20:1 and vibrated by an ultrasonic instrument for 20 min. A few drops of the slurry were then added to a copper grid net by a straw for the TEM tests. The sulfur and oxygen contents in the samples were analyzed by a LECO CS600 and a LECO TCH600L, respectively. The samples were dissolved in a 6 mol/L HCl solution, and the As, Fe and S contents were determined by ICP−MS (Thermo scientific/ XSERIES 2).

2.2.3 Stability testing

For samples S1, S2 and S3, three types of leaching experiments were conducted to evaluate their stability.

Firstly, TCLP tests were conducted at pH 4.93. According to the method produced by the US-EPA [34], a HAc−NaAc buffer solution with pH 4.93 was used as the extraction liquor, and leaching tests were conducted at a liquid/solid mass ratio of 20:1 at (25±1) °C for 60 h.

Secondly, long-term leaching tests were conducted using aqueous solutions containing NaOH, CaO−NaOH, $Mg(OH)_2$, NaH_2PO_4−NaOH, and tap water as extraction liquors. During leaching, the pH of the extraction liquors continuously decreased and was not adjusted artificially. The initial and final pH values of the extraction liquors are shown in Table 1. The tests were conducted at a liquid/solid mass ratio of 20:1 at (25±1) °C for 40 d. CaO and $Mg(OH)_2$ are the most common alkaline substances in nature, while NaOH is the common alkaline substance used in laboratories, and many researchers have used its aqueous form as an extraction liquor to test the stability of scorodite under alkaline conditions [30]. NaH_2PO_4 is used to prepare an alkaline buffer solution [32]. Phosphate is often present in domestic water due to the

Table 1 Composition and pH of leaching extraction liquors at (25±1) °C for 40 d

Extraction liquor	Initial pH	Final pH		
		S1	S2	S3
NaOH	10.05	4.72	4.03	2.60
	8.33	4.66	3.98	2.62
	9.25	4.70	3.87	2.75
CaO−NaOH	10.88	5.32	4.46	3.27
	9.67	5.50	4.41	3.30
	10.16	5.47	4.38	3.28
$Mg(OH)_2$	9.47	4.83	3.91	2.96
NaH_2PO_4−NaOH	7.95	6.87	5.39	5.11
	10.57	7.34	5.88	5.63
	9.69	7.16	5.74	5.61
Tap water	5.40	3.80	3.12	2.73

use of phosphorus-containing detergents. PO_4^{3-} radicals in the extraction liquor would increase the release of arsenic from scorodite as they undergo an "ion exchange" reaction with AsO_4^{3-}, therefore, a phosphate buffer solution was selected to assess the efficacy of coating.

Thirdly, another set of long-term leaching tests were conducted using a NaH_2PO_4−NaOH buffer solution with a pH of 10.5, and NaOH solutions with pH values of 8.6 and 10.0 as extraction liquors. The NaH_2PO_4−NaOH buffer solution was prepared by the dropwise addition of 1 mol/L NaOH into 0.025 mol/L NaH_2PO_4 to adjust the pH to 10.5. The ionic strength of all the three solutions was less than 0.05 mol/kg. The leaching tests were conducted with a liquid/solid mass ratio of 20:1 at (25±1) °C for 30 d, and each test was replicated three times. During the tests, the pH and φ (redox potential) values of the leaching slurry were measured twice per day by using a Mettler Toledo pH and φ instrument, with an Ag/AgCl reference electrode. The pH of the leaching slurry continuously decreased, thus, the pH was maintained at the initial value by the dropwise addition of a 0.1 moL/L NaOH solution at the same time that each pH measurement was taken.

The concentrations of arsenic, iron and sulfur in the leaching solutions were determined by ICP−AES.

3 Results and discussion

3.1 Phenomenon description and extension of arsenic precipitation

During synthesis, a clear precipitate appeared immediately after the first drop of the ferrous sulfate solution was added to the arsenate solution, but the precipitate disappeared immediately with stirring. Approximately 5 min later, a white precipitate formed in the solution, which did not disappear with stirring. Approximately 15 min after the precipitate appeared, it turned light green in color, which darkened to green within approximately 40 min. The color of the precipitate did not change after this.

Figure 3 shows the arsenic concentration in the solution and the extent of arsenic precipitation as a function of the synthesis reaction time. From Fig. 3, it can be seen that, during synthesis, As(V) ions were precipitated completely within 1 h when the initial Fe/As molar ratio was 2:1 or 3:1, while they precipitated completely within almost 2 h when the initial Fe/As molar ratio was 1:1. After arsenic precipitation completed, the slurry was aged until the reaction time reached 7 h.

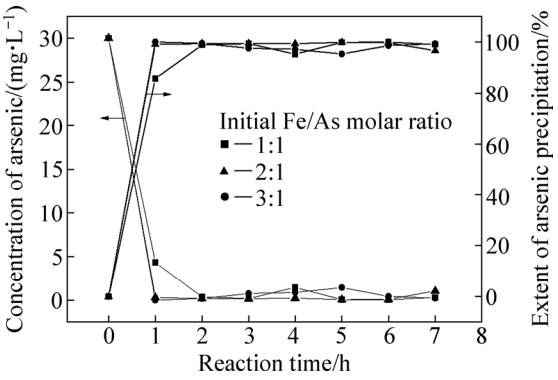

Fig. 3 Concentration of arsenic in solution and extent of arsenic precipitation as function of reaction time

3.2 Characterization of synthesized samples

3.2.1 Chemical composition

The chemical compositions of the three synthesized samples are shown in Table 2. Based on its chemical formula ($FeAsO_4·2H_2O$), scorodite theoretically contains 32.47 wt.% As, 24.24 wt.% Fe, and 41.56 wt.% O. However, the actual chemical composition of scorodite, whether it is natural or synthetic, may deviate from its theoretical value due to the substitution of sulfate or hydroxyl for arsenate in its lattices, or the coexistence of a secondary phase in samples. From Table 2, the chemical compositions of all three samples deviated noticeably from the theoretical scorodite composition, with lower arsenic and higher iron contents, and the Fe/As molar ratio exceeded 1:1. Moreover, there was some sulfur in all three samples. From S1 to S3, the iron and sulfur contents, as well as the Fe/As molar ratio, increased, while the arsenic and oxygen contents decreased initially before increasing. For S2 and S3, the obvious deviation of their Fe/As molar ratios from the theoretical value of 1:1 suggests that the samples may include another iron-containing phase. According to the above analysis, the iron phase formed through hydrolysis

Table 2 Chemical compositions of samples

Sample	Content/wt.%				Fe/As molar ratio
	As	Fe	O	S	
S1	31.50±0.03	25.30±0.03	41.35±0.03	0.17±0.01	1.078:1
S2	29.58±0.02	25.68±0.01	38.48±0.02	0.74±0.01	1.165:1
S3	29.66±0.03	27.69±0.01	39.17±0.02	1.08±0.01	1.252:1
Theoretical value	32.47	24.20	41.60	0	1:1

and precipitation of ferric irons in the solution. Thus, it can be inferred that this phase may contain iron oxides, iron hydroxides, ferrihydrite, basic iron sulfates, or iron hydroxide-containing sulfates. For the sake of simplicity, these compounds are collectively described as "iron (hydr)oxide" in this work.

3.2.2 XRD patterns

From the XRD patterns of the synthesized samples (Fig. 4), all major peaks in the patterns of S1, S2, and S3 were consistent with the characteristic XRD peaks of scorodite (JCPDS-ICDD No. 37−0469) and showed a narrow, tall shape, indicating that the main phase of all three samples was high-crystallinity scorodite. The two strongest peaks of S1, S2, and S3 (111 and 200) were compared by overlapping the patterns, as shown in the upper right corner of Fig. 4. The peak intensities and full width at half maximum (FWHM) of S1 and S2 were higher and narrower than those of S3, suggesting that they were more crystalline. According to the analysis for chemical composition of the samples, iron (hydr)oxide formed when the initial Fe/As molar ratio exceeded 1:1. Therefore, it can be speculated reasonably that the iron (hydr)oxide affected the XRD pattern and decreased the crystallinity of products.

3.2.3 SEM observation

From the SEM images of the synthesized samples (Fig. 5), the particle sizes of S1 to S3 tended to decrease gradually, from 5−10 μm in S1 to 3−4 μm in S3. It can also be seen that there were two different types of particle morphologies in the samples, which were polyhedral and raspberry-like.

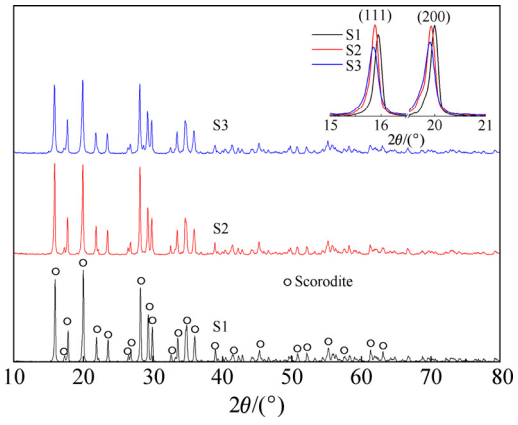

Fig. 4 XRD patterns of S1, S2 and S3

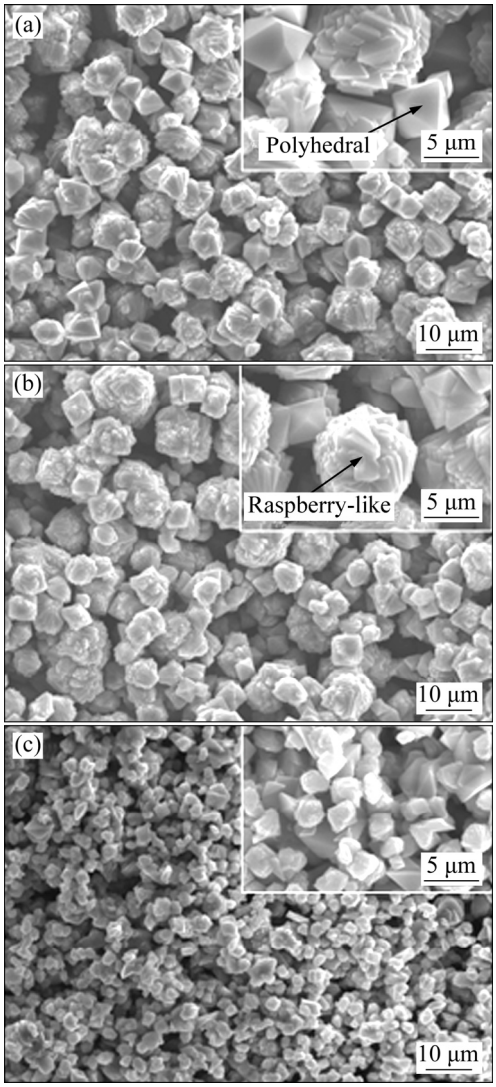

Fig. 5 SEM images of S1 (a), S2 (b) and S3 (c)

From the experimental phenomenon described in Section 2.1, the ferrous ions added into the system were firstly oxidized into ferric ions, which then combined chemically with the arsenate in the system to precipitate as scorodite. The process can be described by following equations:

$$Fe^{2+}+1/4O_2+H^+=Fe^{3+}+1/2H_2O \quad (2)$$

$$Fe^{3+}+H_3AsO_4+2H_2O=FeAsO_4\cdot 2H_2O+3H^+ \quad (3)$$

The rate of Reaction (2) was relatively slow [38]. Therefore, the initial Fe/As molar ratio determines the

supersaturation of scorodite precipitation during synthesis; the higher the initial Fe/As molar ratio is, the larger the scorodite precipitation supersaturation is. That is, from S1 to S3, the supersaturation of scorodite precipitation increases.

When an insoluble compound precipitates from a solution, particle formation involves two fundamental processes: nucleation and growth; the driving force for both of these is the supersaturation of the insoluble compound. As described in the LaMer model [39], the supersaturation required for the nucleation is much higher than that required for growth. It can be deduced that, during precipitation, the higher the supersaturation is, the greater the nuclei formation is. Therefore, during synthesis, the number of scorodite nuclei would continue to increase from S1 to S3 with the increase in scorodite precipitation supersaturation, thus gradually decreasing the sizes of the scorodite particles in the samples.

Both particle morphologies formed through nucleation and growth, but their formation mechanisms were slightly different. Scorodite crystals are orthorhombic system, and commonly possess pyramidal (111) (sometimes, pseudo-octahedral), tabular (001), and prismatic (010) morphologies [40]. From Fig. 5, the polyhedron-like particles in the samples are pyramidal, which are of a typical scorodite morphology. The polyhedral particles formed through a primary nucleation-orderly growth mechanism, which is a homogeneous process that occurs at a higher supersaturation. The raspberry-like particles formed through a composite process consisting of both primary and secondary nucleation-growth, which is a heterogeneous process on the surfaces of the crystals that previously formed at a lower supersaturation. During synthesis, the formation and growth of secondary nuclei result in the disordered growth of scorodite particles [41,42], which is the formation mechanism of raspberry-like particles. The spatiotemporal heterogeneity of scorodite precipitation supersaturation is the reason for the formation of two different types of particles with different morphologies.

3.2.4 TEM and HRTEM observation

To investigate the structure of the synthesized sample, TEM characterization was conducted for S2 with a probe size of approximately 50 nm at 200 kV. Figure 6 shows the bright field TEM images of a raspberry-like particle from S2. As shown in Fig. 6(a), the particle was approximately 4 μm in size. The area circled with a red dashed line at the top right-hand corner of the particle was scanned into a high-definition image, as shown in Fig. 6(b). From Fig. 6(b), large amounts of microcrystalline grains gathered as an agglomerate, and some were present as regular polyhedrons [43]. Two typical grains were projected hexagonally in the image, which are indicated by red numbers 1 and 2. A magnified image of the two grains is shown in Fig. 6(c). According to the geometry calculation, Fig. 6(c) presents the overlap of the two hexagons, the side length of them is 32 nm. According to crystalline symmetry, the hexagon corresponds to a hexagonal bipyramid. Therefore, the two bipyramids formed through an overlap at a corner. This structure is representative of typical self-similarity inside scorodite particles. As a large amount of the structures were particulate, raspberry-like particles formed.

Figure 7 shows the bright field TEM and HRTEM images of S1. A part of raspberry-like particle was presented in Fig. 7(a). A spot circled with dash-red line at the bottom edge of the particle was selected for HRTEM testing. Figure 7(b) shows the HRTEM image of the spot. It can be seen that lots of crystalline lattice fringes were present, and the interplanar spacing was determined to be 3.04 Å, corresponding to the crystal face (131) of scorodite. The results of elemental content analysis by TEM−EDX are shown in Table 3. It indicates that the Fe/(As+S) molar ratio was 0.95±0.06, corresponding to the theoretical value of scorodite. Therefore, S1 can be determined as pure scorodite.

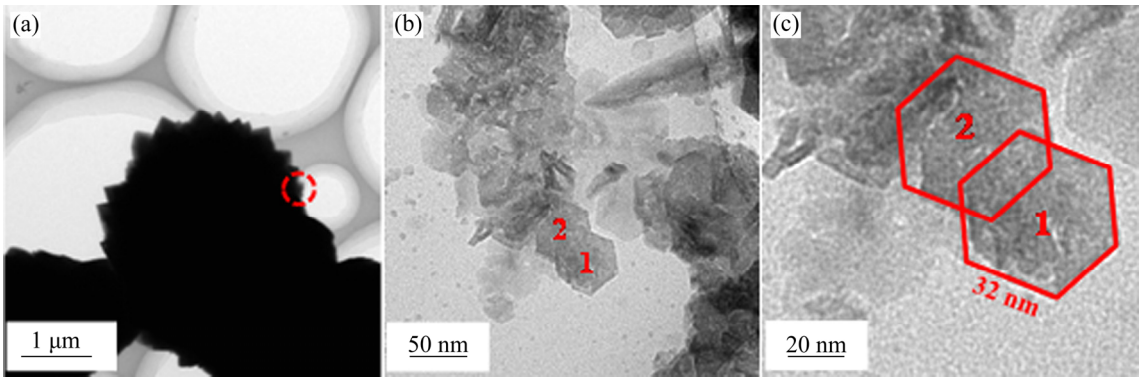

Fig. 6 Bright field TEM images of S2: (a) TEM image of one particle for S2 (the area circled with dot-red line was used for high-definition scan); (b) High-definition image of corner of particle indicated with dot-red line in (a); (c) Structural model for crystalline grains indicated with red numbers in (b)

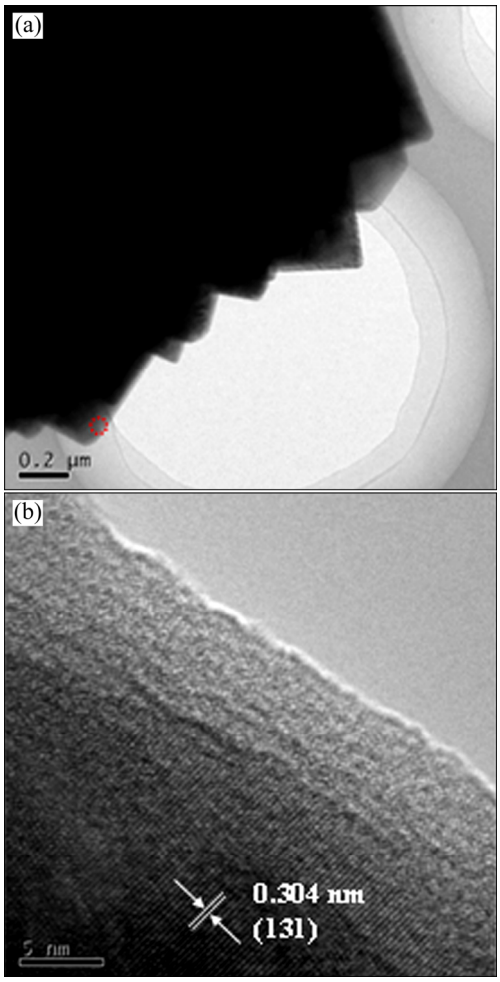

Fig. 7 Bright field TEM and HRTEM images of S1: (a) TEM image of scorodite particle (the spot indicated with dot-red circle was used for HRTEM); (b) HRTEM image of spot indicated in (a)

Table 3 Results of TEM−EDX characterization for spot indicated with dot-red circle shown in Fig. 7

Content/at.%				Fe/(As+S) molar ratio
Fe	As	S	O	
14.01±0.38	14.73±0.55	0.11±0.05	71.24±0.60	0.95±0.06

Figure 8 shows the bright field TEM and HRTEM images of S3. Two spots at the edge of a 2 μm particle from S3 were selected for testing (Fig. 8(a)). In Spot 1, there was no crystalline lattice fringe (Fig. 8(b)), and the fast Fourier transformation (FFT) image showed that only amorphous material was present. The composition of Spot 1 was tested by TEM−EDX. The Fe/(As+S) molar ratio of was 1.625±0.184 (Table 4); theoretically, even though a small amount of SO_4^{2-} replaced some of the arsenate atoms in the scorodite, the Fe/(As+S) molar ratio should be equal to 1. It can be concluded that there were excess iron and oxygen atoms in the sample, which might be sulfur-containing iron (hydr)oxide compounds formed through the hydrolysis of ferric ions. In Spot 2, there was a crystalline lattice fringe surrounded by amorphous material (Fig. 8(c)), and the light spots that indicate the crystal faces are shown in Fig. 8(d). The interplanar spacing was 4.083 Å (Fig. 8(d)), which corresponded to the crystal face (201) of scorodite [44]. The TEM−EDX assessment of Spot 2 showed that the Fe(As+S) molar ratio was 1.125±0.075 (Table 4). To estimate the thickness of the coating layer, an approximate calculation using the iron contents of the above two spots was proposed. The particle was assumed to be spherical, with a diameter of 2 μm, and the excess precipitated iron was assumed to uniformly coat the scorodite. The total iron content was 100%, and it exhibited constant and equal density in the scorodite and coating layer. An Fe/(As+S) molar ratio of 1.625±0.184 was measured at Spot 1, and the iron contents in scorodite and the coating were 61.5% and 38.5%, respectively. The thickness of the coating was calculated by a simple mathematical operation and found to be 350 nm. The same method was followed for Spot 2, and the thickness of the coating was 80 nm. Therefore, from characterization and calculations, the scorodite particle was nonuniformly coated with a high sulfur-containing iron (hydr)oxide compound, with a thickness ranged from tens to hundreds of nanometers.

3.2.5 STEM observation

To characterize the coating layer of S3 more directly, STEM−EDS was conducted at 300 kV with a probe size of 0.2 nm in a high-angle annular dark field (HAADF). Figure 9 presents the HAADF image; Fe (K_α), As (K_α), and S (K_α) elemental mapping; and the EDS spectrum of a 2−3 μm, raspberry-like particle from S3. The HAADF image of the particle is presented in Fig. 9(a), which showed that the particle was thinner at the edges than it was in the middle. The Fe, As and S mapping images of the particle are presented in Figs. 9(b), (c) and (d), respectively. The distributions of elements Fe, As and S were congruent, therefore, an iron (hydr)oxide coating layer cannot be identified from the image. The EDS spectrum of the particle is presented in Fig. 9(e), showing that the mole fractions of Fe, As and S in the sample are 52.45%, 44.73% and 1.36%, respectively (see Table 5). The Fe content was higher than that of As, which was consistent with the chemical composition (Section 2.1). Additionally, the presence of C and Cu on the spectrum was caused by the carbon film and copper grid net that were used during characterization. The Na present on the spectrum was there to verify if the coating was composed of Na-jarosite ($NaFe_3(OH)_6(SO_4)_2$). However, there was no elemental Na in the sample as indicated by its extremely low intensity on the spectrum; thus, Na-jarosite could be excluded. Figs. 9(a_1) and (a_2)

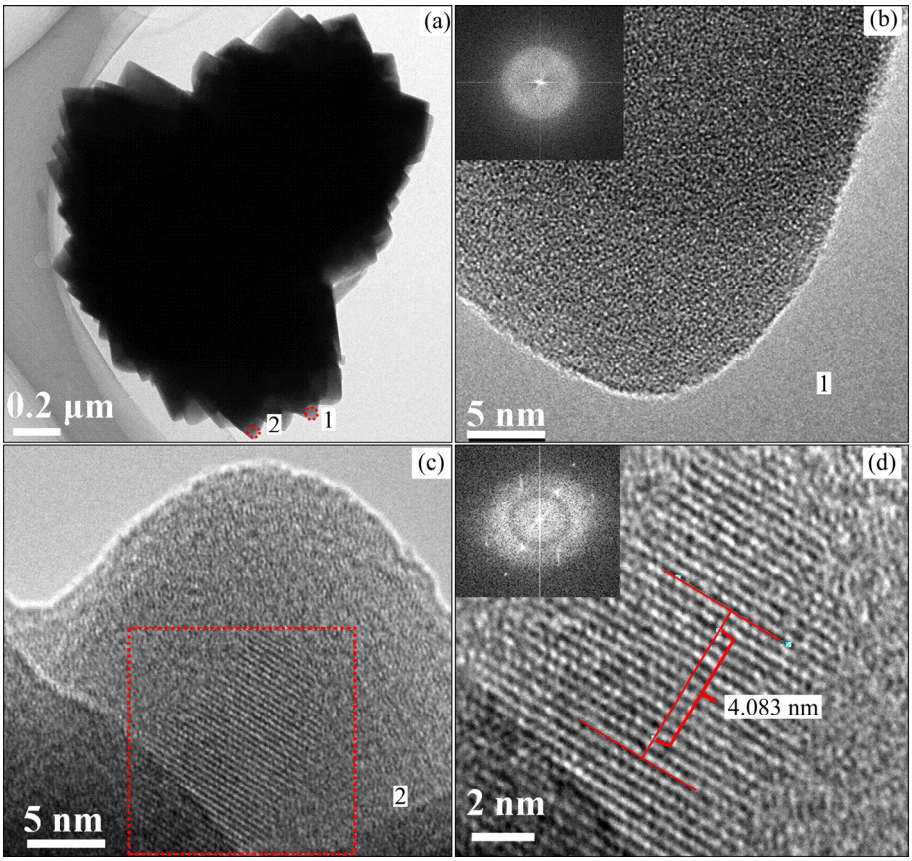

Fig. 8 Bright field TEM and HRTEM images of S3: (a) TEM image of scorodite particle (Spots 1 and 2 signed by numbers in image were used for HRTEM and TEM−EDX measurement); (b) HRTEM and FFT images of Spot 1 indicated in (a); (c) HRTEM image of Spot 2 indicated in (a); (d) Amplification and FFT image of area surrounded by dot red line in (c) (Ten lattice fringes were selected to determine the interplanar spacing)

Table 4 Results of TEM−EDX characterization for spots indicated with dot-red circle shown in Fig. 8

Spot	Content/at.%				Fe/(As+S) molar ratio
	Fe	As	S	O	
1	17.38±0.38	10.76±0.63	0.29±0.05	71.54±0.76	1.625±0.184
2	15.73±0.38	12.91±0.49	1.06±0.06	70.2±0.55	1.125±0.075

are the amplified images of two particle edge areas, indicated by red numbers 1 and 2 in Fig. 9(a). The mapping images of Fe, As and S in Areas 1 and 2 in Fig. 9(a) are shown in Figs. 9(b_1−d_1) and 9(b_2−d_2), respectively. The mapping of both areas indicated that the content of Fe was much higher than that of As. The mole fraction of As was as low as 0.42%, and that of Fe reached 63.56%. Therefore, it can be concluded that the main material on the edge of the particle was an iron-containing compound. However, the mole fraction of S in Area 2 reached 37.44%, which greatly exceeded the S content of the whole particle (1.36%). This suggested that S mainly existed in the coating layer as SO_4^{2-}. Spot and linear scans of another randomly-selected 3 μm particle are presented in Fig. 10(a), in which the positions of spots were indicated by red numbers, and the linear scan was conducted along with the green line. The results of the spot scans are summarized in Table 6, which demonstrated that the Fe/As molar ratio at the center of the particle was almost 1:1, however, that of Spots 3 and 4 on the edge far exceeded 1:1, which was consistent with the maps of Areas 1 and 2 in Fig. 9(a). The distributions of Fe, As and S along the green line in Fig. 10(a) are presented in Fig. 10(b), which showed that the content of Fe was much higher than that of As within a certain thickness on the surface of the S3 particle, and, through scanning, the As content increased noticeably and the slopes of the relative intensity curve for both Fe and As were consistent. The results of the linear scan further validated that, for S3, there was an iron (hydr)oxide coating layer on the surface of the scorodite.

To preliminarily determine the structure and composition of the coating layer, simple calculation and reasoning processes were proposed, based on the STEM characterization results of S3. The data used for calculation were the elemental contents, which are shown in Tables 5 and 6. For the data regarding position 3 in Table 6 (~63.25 at.% Fe, ~2.35 at.% As, ~34.40 at.% S), the arsenic originated from scorodite, with an Fe/As molar ratio of 1:1. Thus, the relative content of Fe in the coating was 60.9%, giving an Fe/S molar ratio of 1.77:1. In the sample, S existed as SO_4^{2-} because the sample was synthesized in a sulfate system.

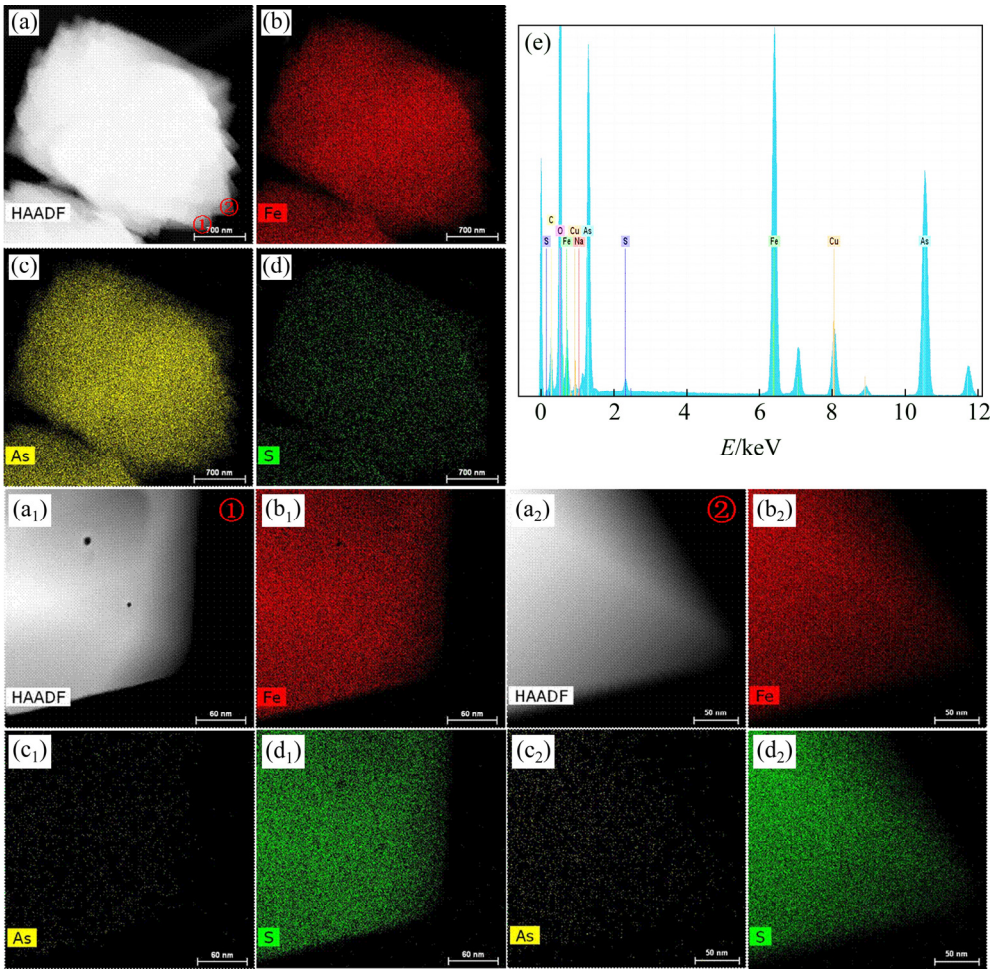

Fig. 9 STEM−EDS elemental mapping of S3: (a) HADDF image of particle; (b−d) Fe, As and S (K_α) EDS mapping images of particle, respectively; (e) EDS spectrum of particle; (a_1) HADDF image of Area 1 indicated with red number in (a); (b_1−d_1) Fe, As and S (K_α) EDS mapping images of Area 1, respectively; (a_2) HADDF image of Area 2; (b_2−d_2) Fe, As and S (K_α) EDS mapping images of Area 2, respectively

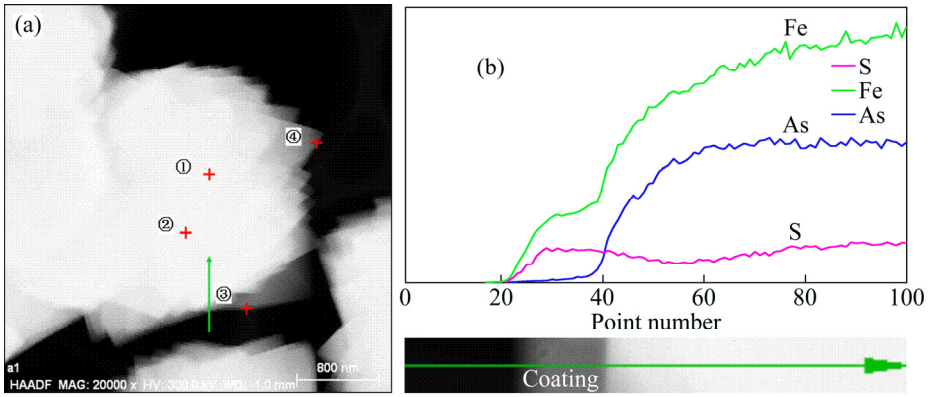

Fig. 10 STEM−EDS spot scan and line profiles of S3: (a) Position of spots and linear scan; (b) Line profiles

Table 5 Elemental contents obtained from STEM−EDS mapping shown in Fig. 9

Position	Content/at.%		
	Fe	As	S
Particle	52.45	44.73	1.36
Area 1	63.56	0.42	36.02
Area 2	62.00	0.56	37.44

Table 6 Elemental contents obtained from STEM−EDS spot scan shown in Fig. 10

Position	Content/at.%			Fe/As molar ratio
	Fe	As	S	
1	49.30	49.66	1.05	0.99:1
2	50.76	40.76	8.48	1.25:1
3	63.25	2.35	34.40	26.91:1
4	61.37	3.28	35.35	18.71:1

In addition, the coating was formed by the hydrolysis of ferric ions, so it could have contained a great amount of —OH groups, with some crystals or adsorbed water. Therefore, the molecular formula of the coating could be $Fe_{1.77}(OH)_x(SO_4)\cdot aH_2O$, and according to the conservation of charge, the "x" could be 3.31. The molecular formula was $Fe_{1.77}(OH)_{3.31}(SO_4)\cdot aH_2O$, and, after normalization, the molecular formula can be written as $Fe(OH)_{1.88}(SO_4)_{0.56}\cdot aH_2O$. The data of Areas 1 and 2 in Table 5 and Position 4 in Table 6 were processed in the same manner to determine the vibration range of the formula. From the results, it can be concluded that the molecular formula of the coating was $Fe(OH)_x(SO_4)_y\cdot aH_2O$, where the limiting conditions were $1.78\leq x\leq 1.88$, $0.56\leq y\leq 0.61$, $x+2y=3$, and "a" was a positive number. In accordance with previous work [45,46], the structure could belong to the basic iron sulfate or hydronium jarosite subspecies, or be precursor of polyferric sulfate. It is noticed that, the presence of hydrogen and oxygen radicals was ignored, so the potential structure of $H_mFeO_n(OH)_x(SO_4)_y\cdot aH_2O$ could not be excluded.

3.3 Stability

3.3.1 TCLP tests

TCLP tests were conducted at pH 4.93 for 60 h for the three prepared samples, and the results are presented in Fig. 11(a). The arsenic concentration in the leaching solution of S1 was 7.18 mg/L, which greatly exceeded that specified in both the standards of China and USA [34,47]. However, the arsenic concentrations for S2 and S3 were 0.19 and 0.12 mg/L, respectively, which were far below the standards. This is because the arsenic leaching of scorodite was effectively postponed by the iron (hydr)oxide coating.

3.3.2 Long-term leaching using various extraction liquors

Long-term (40 d) leaching tests were conducted using aqueous solutions that contained different chemicals (NaOH, CaO−NaOH, $Mg(OH)_2$ and NaH_2PO_4−NaOH) and tap water as extraction liquors, with initial pH values ranging from 5.40 to 10.88 (Table 1). The results of the leaching tests are shown in Figs. 11(b−g). From Figs. 11(b) and (c), it can be seen that, as the Fe/As molar ratio in the precipitates increased, the leaching stability of the samples was improved. For S1, all released arsenic concentrations exceeded the 1 mg/L standard. However, for S3, the arsenic concentrations in the leaching solutions decreased noticeably and were all below 0.5 mg/L. The arsenic concentrations in seven of these experiments (NaOH with initial pH of 10.05, 8.33, and 9.25; CaO−NaOH with initial pH of 9.67; NaH_2PO_4−NaOH with initial pH of 10.57 and 9.69; and tap water with pH of 5.40) were below 0.01 mg/L. In contrast, the leaching concentrations of iron and sulfur increased as the Fe/As molar ratio in the precipitates increased (Figs. 11(d−g)). From S1 to S3, the concentrations of iron and sulfur increased from approximately 0.05 to 10 mg/L and 3 to 60 mg/L, respectively. The high concentrations of iron and sulfur in the solution could only originate from the coating, which suggested that it was not stable and decomposed in the leaching solutions. All the final pH values of the extraction liquors were much lower than their initial values, indicating that the pH continuously decreased during the leaching tests. For S1, the pH decreased from the alkaline to acidic ranges, which was attributed to the release of iron from scorodite that would combine with the abundant hydroxyl ions, producing $Fe(OH)_3$ and $Fe(OH)_4^-$ [48]. However, for S3, the decrement of pH was greater as a higher concentration of iron was released from the coating. According to the scorodite incongruent dissolution theory [48], when the pH was above 2.0, the released iron ions precipitated as $Fe(OH)_3$ and FeOOH, which then coated the surface of scorodite particles [37]. Similarly, in our study, the iron (hydr) oxide coating dissolved and was also converted to $Fe(OH)_3$ and FeOOH. Furthermore, ZHU and MERKEL [22] found that the solubility of scorodite decreased when it was present in a solution with $Fe(OH)_3$, due to a dissolution−precipitation equilibrium between $Fe(OH)_3$ and scorodite. This may be the reason causing the low concentration of released arsenic in S3.

3.3.3 Long-term leaching using NaH_2PO_4−NaOH buffer solution and NaOH solution

Figure 12 shows the leaching concentrations of arsenic, iron and sulfur as a function of reaction time from the long-term (30 d) leaching tests of S1 and S3 using NaH_2PO_4−NaOH buffer solution. The initial pH of

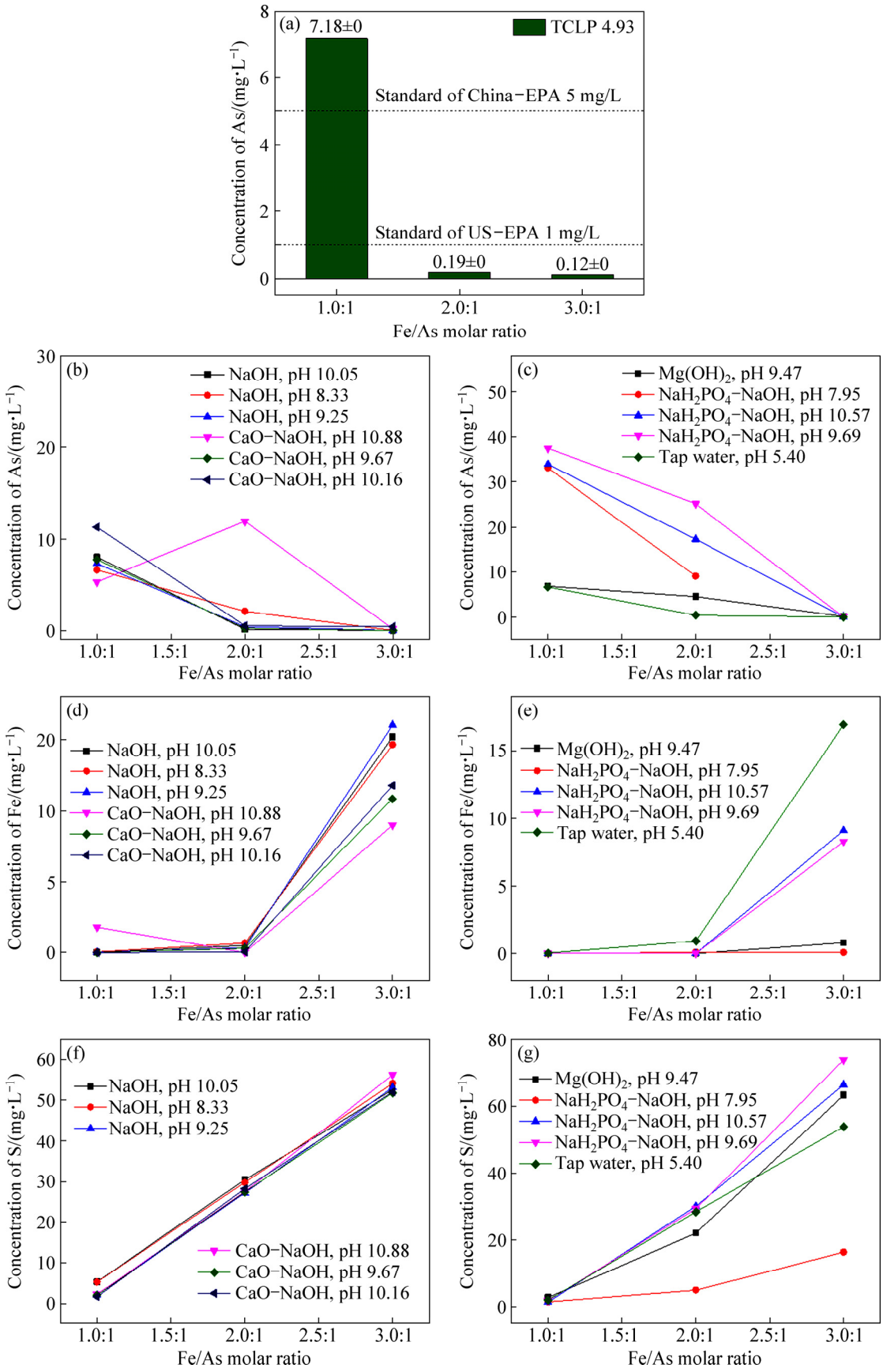

Fig. 11 Concentrations of As from TCLP of pH 4.93 (a) and concentrations of As (b, c), Fe (d, e) and S (f, g) from leaching test of 40 d with weak acidic to alkaline solutions at about 25 °C

the solution was maintained at 10.5; however, as leaching continued, the pH kept continued to decrease due to the release of iron that combined with hydroxyl groups in the solution. Within the first 6 d of leaching, the pH decreased to 8.8. We intended to test the stability of the samples under a constant pH. Therefore, the solution was adjusted back to its initial pH from the sixth day. The φ of the solution was also measured during the leaching tests, which fluctuated within a range of 40−180 mV, indicating that leaching occurred under weakly reductive conditions. From Fig. 12(a), the concentration of arsenic released from S3 was much lower than that from S1. The concentration of arsenic in S1 continued to increase linearly, and it reached 93 mg/L on the 30th day; however, for S3, the leaching concentration only slightly increased; it was below 1.0 mg/L prior to the 17th day, and, at the end of leaching, the concentration of arsenic was 1.3 mg/L, which was slightly higher than the standard set by the US−EPA. From Figs. 12(b) and (c), the average leaching concentration of iron released from both S1 and S3 was approximately 0.5 mg/L, and it continuously increased without becoming saturated; the concentration of sulfur released from S1 was maintained below approximately 0.01 mg/L, however, that released from S3 increased linearly to 33.5 mg/L on the 30th day. This suggested that sulfur was mainly released from the scorodite coating in S3, and also indicated that it decomposed.

Figure 13 shows the results of long-term (30 d) leaching tests, which used NaOH solutions with pH values of 8.6 (Figs. 13(a−c)) and 10.0 (Figs. 13(d−f)). For the pH 8.6 leaching solution, Fig. 13(a) shows that the concentrations of arsenic released from S3 were much lower than those released from S1. As leaching continued, the concentrations of arsenic released from S3 remained at approximately 0.1 mg/L. However, the concentration of arsenic released from S1 continued to increase, with an average value of 2.9 mg/L. However, the concentrations of iron and sulfur released from S1 were much lower than those released from S3 (Figs. 13(b) and (c)), which were as low as 1.5 and 2.8 mg/L, respectively. However, for S3, the concentrations of iron and sulfur increased noticeably during on the 5th day, and then increased to approximately 43.4 and 75.9 mg/L, respectively. There were almost no differences in the overall trends for the pH 10.0 leaching solution. From Fig. 13(d), the concentration of arsenic released from S3 remained at approximately 0.5 mg/L, but that released from S1 increased continuously and reached 4.2 mg/L on the 30th day. The behavior of iron and sulfur in the pH 10.0 solution was the same as that in the pH 8.6 solution. On the 5th day, the concentrations of iron and sulfur released from S3 increased to 57.2 and 96.2 mg/L, respectively, and then plateaued, while those from S1

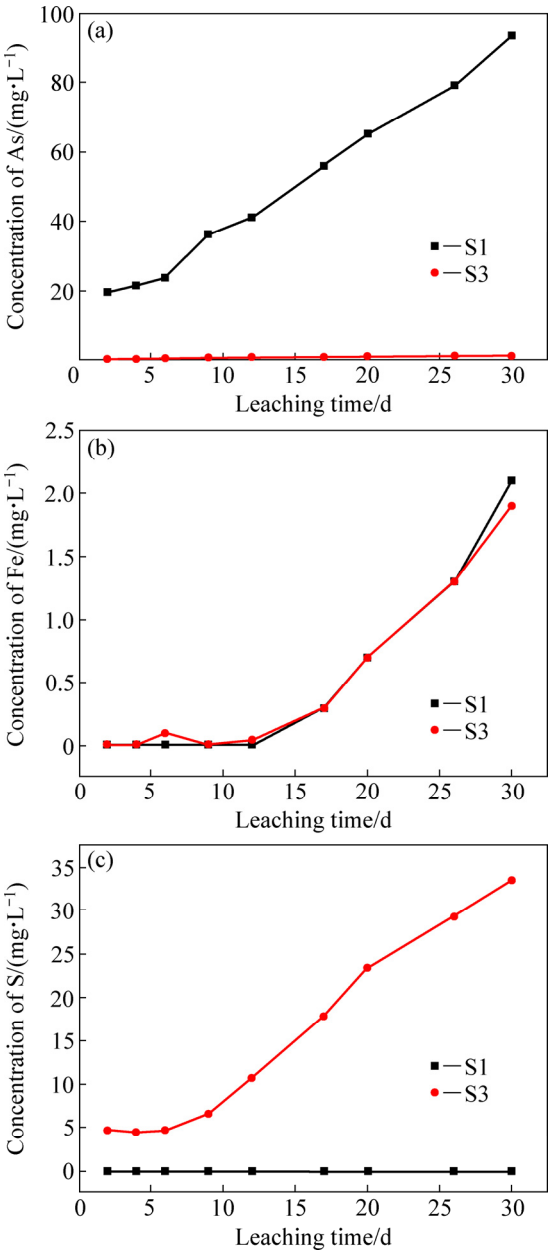

Fig. 12 Leaching concentrations of As (a), Fe (b) and S (c) from consecutive leaching tests of S1 and S3 by NaH_2PO_4–NaOH buffer solution with adjustive pH of 10.5 at about 25 °C

were much lower, reaching approximately 2.0 and 11.0 mg/L, respectively, on the 30th day. The high concentrations of iron and sulfur released from S3 originated from the coating, indicating that it continuously decomposed, which was consistent with the results using the NaH_2PO_4–NaOH buffer. However, the difference between the concentrations of iron and sulfur released from S3 during the leaching tests using NaH_2PO_4–NaOH and NaOH solutions was that the former exhibited non-saturation, but the latter exhibited saturation. This may be because ferric ions in NaOH solutions hydrolyze and precipitate as $Fe(OH)_3$, while

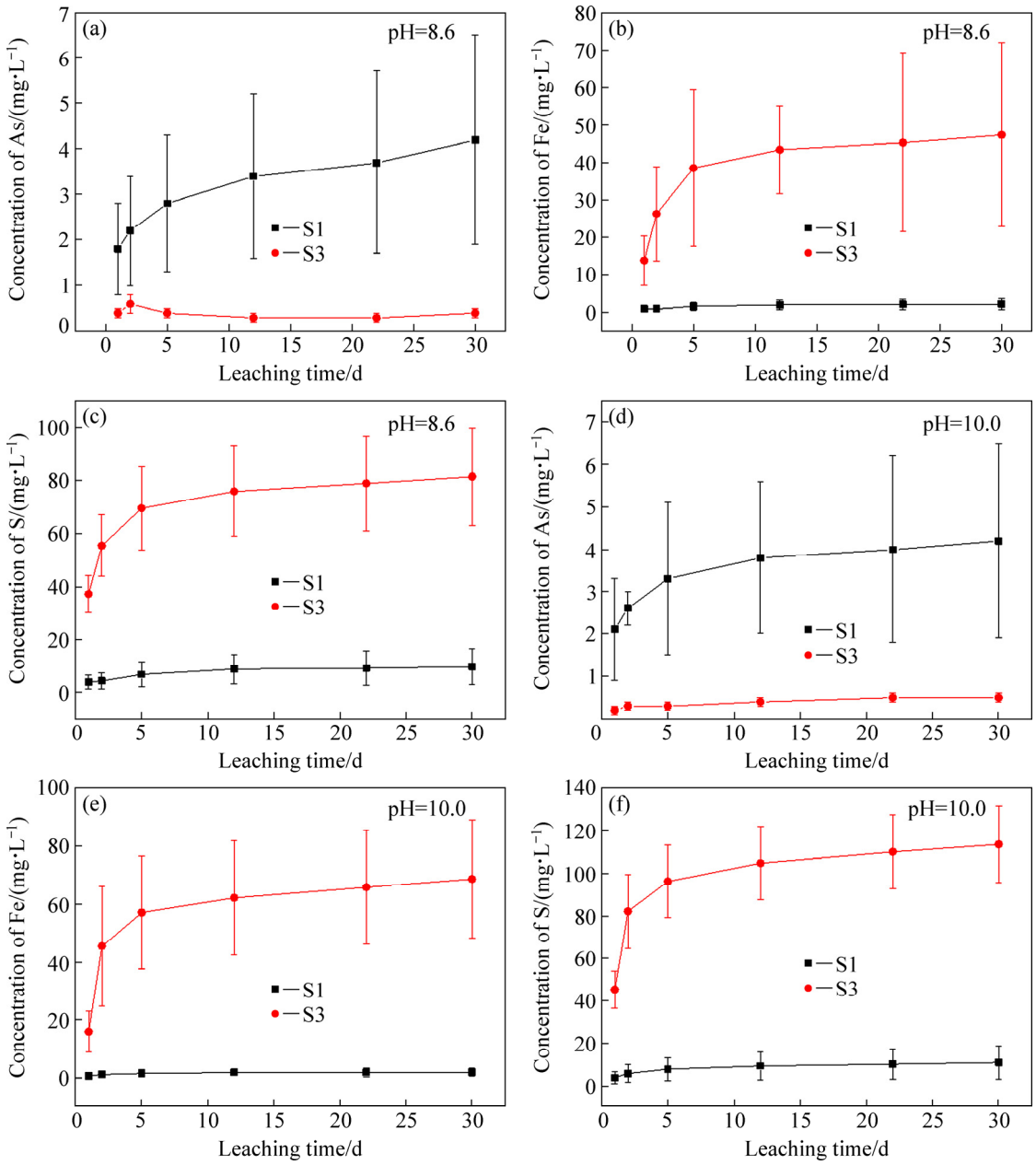

Fig. 13 Leaching concentrations of As (a, d), Fe (b, e) and S (d, f) from consecutive leaching tests of S1 and S3 by NaOH solutions with adjustive pH values of 8.6 (a−c) and 10.0 (d−f) at about 25 °C for 30 d

this reaction is restricted in NaH_2PO_4–NaOH solutions. The mechanism behind this is not fully understood. The φ of the leaching solution during the tests fluctuated within a range of 260−420 mV, indicating that the leaching tests were conducted in an oxidizing environment. The standard deviations of the arsenic ($C_{As,Std.}$), iron ($C_{Fe,Std.}$), and sulfur ($C_{S,Std.}$) concentrations released from S1 in the pH 8.6 NaOH solution were approximately 1.8, 1.4 and 5.6 mg/L, respectively, and those from S3 were approximately 0.1, 18.0 and 16.0 mg/L, respectively. However, $C_{As,Std.}$, $C_{Fe,Std.}$, and $C_{S,Std.}$ released from S1 in the pH 10.0 NaOH solution were approximately 1.8, 1.1 and 6.6 mg/L, respectively, and those from S3 were approximately 0.1, 19.7 and 17.3 mg/L, respectively.

The overall concentrations of arsenic from S1 in the NaH_2PO_4–NaOH buffer solution greatly exceeded those in the NaOH solution, and increasing trends greatly differed. This was because the PO_4^{3-} radicals in the solution would exchange with the AsO_4^{3-} radicals in scorodite under alkaline conditions, thereby increasing the release of arsenic [32]. Additionally, under the reductive conditions of the NaH_2PO_4–NaOH buffer solution, scorodite was much less stable than that under the oxidative conditions of NaOH solutions, which has been reported previously [25]. However, the

concentrations of arsenic released from S3 in above two solutions were almost at the same low-value and the only cause of arsenic release was the behavior of the coating.

In summary, for S3, the release of arsenic under both the NaH_2PO_4−NaOH buffer and NaOH solutions was restricted by the iron (hydr)oxide coating, which continuously decomposed during the leaching tests. Two mechanisms were proposed based on the results. Firstly, the scorodite particles were coated with iron (hydr)oxide, which slowed the dynamic leaching process, and secondly, during scorodite dissolution, a dissolution−precipitation equilibrium between the iron hydroxides and scorodite was maintained, therefore, when iron (hydr)oxide is present alongside scorodite, arsenic dissolution decreased noticeably. The combined effect of the above two mechanisms controlled the release of arsenic.

4 Conclusions

(1) High crystallinity scorodite with a high leaching stability was prepared by introducing an oxidizing gas into a reaction mixture containing ferrous sulfate and arsenic, to convert ferrous to ferric ions. A sodium carbonate solution was added to neutralize the protons released by this reaction and stabilize the reaction rate. The synthesized scorodite particles exhibited polyhedral and raspberry-like morphologies, and were 5−10 or 3−4 μm in size, respectively, depending on the initial Fe/As molar ratio.

(2) The inclusion of SO_4^{2-} increased as the initial Fe/As molar ratio increased. From the TEM, HRTEM and STEM characterizations, it was found that, when the initial Fe/As molar ratio was 3:1, excessive ferric ions would precipitate as iron (hydr)oxides that contained sulfate and coated the surface of the scorodite particles. Through conducting calculation and reasoning processes, the chemical phase of the coating was determined to be basic iron sulfate, hydronium jarosite, or a precursor of polyferric sulfate.

(3) From the results of the leaching tests, scorodite with an iron (hydr)oxide coating was more stable than scorodite. For sample S3 prepared at an initial Fe/As molar ratio of 3:1, the lowest concentration of arsenic in the solution was 0.12 mg/L in the TCLP test, and it was below 0.5 mg/L during the long-term leaching tests by the alkaline extraction liquors. The stability of S3 was attributed to the effect of the coating, and the mechanism of this was because the dynamic scorodite leaching process was postponed by the coating, or because the solubility of scorodite decreased due to a new dissolution−precipitation equilibrium between the iron hydroxides and scorodite.

References

[1] NEIL C W, JUN Y S. Fe^{3+} addition promotes arsenopyrite dissolution and iron(III) (hydr)oxide formation and phase transformation [J]. Environmental Science and Technology Letter, 2016, 3(1): 30−35.

[2] WEBSTER T M, REDDY R R, TAN J Y, NOSTRAND N J D V, ZHOU J Z, HAYES K F, RASKIN L. Anaerobic disposal of arsenic-bearing wastes results in low microbially mediated arsenic volatilization [J]. Environmental Science and Technology, 2016, 50(20): 10951−10959.

[3] HOPKIN W. The problem of arsenic disposed in non-ferrous metals production [J]. Environmental Geochemistry and Health, 1989, 3−4(11): 101−112.

[4] KATRIN E, CHRISTIAN M, RUBEN K. Effects of manganese oxide on arsenic reduction and leaching from contaminated floodplain soil [J]. Environmental Science and Technology, 2016, 50(17): 9251−9261.

[5] WANG S L, MULLIGAN C N. Natural attenuation processes for remediation of arsenic contaminated soils and groundwater [J]. Journal of Hazardous Materials, 2006, 138(3): 459−470.

[6] FILIPPOU D, DEMOPOULOS G P. Arsenic immobilization by controlled scorodite precipitation [J]. JOM, 1997, 49(12): 52−55.

[7] RIVEROS G, UTIGARD T A. Disposal of arsenic in copper discharge slags [J]. Journal of Hazardous Materials, 2000, 77(1−3): 241−252.

[8] XIU Wei, GUO Hua-ming, SHEN Jia-xing, LIU Shuai, DING Su-su, HOU Wei-guo, MA Jie, DONG Hai-liang. Stimulation of Fe(II) oxidation, biogenic lepidocrocite formation, and arsenic immobilization by *pseudogulbenkiania Sp.* strain 2002 [J]. Environmental Science and Technology, 2016, 50(12): 6449−6458.

[9] BOLANZ R M, MARIA W W, MARIA C, UHLIK P, GOTTLICHER J, STEININGER R, MAJZLAN J. Structural incorporation of As^{5+} into hematite [J]. Environmental Science and Technology, 2013, 47(16): 9140−9147.

[10] FUJITA T, TAGUCHI R, ABUMIYA M, MATSUMOTO M, SHIBATA E, NAKAMURA T. Novel atmospheric scorodite synthesis by oxidation of ferrous sulfate solution: Part I [J]. Hydrometallurgy, 2008, 90: 92−102.

[11] MOON D H, DERMATAS D, MENOUNOU N. Arsenic immobilization by calcium−arsenic precipitates in lime treated soils [J]. Science of the Total Environment, 2004, 330(1): 171−185.

[12] ROBINS R G, TOZAWA K. Arsenic removal from gold processing waste waters: The potential ineffectiveness of lime [J]. Canadian Mining Metallurgy Bulletin, 1982, 840(75): 171−174.

[13] NISHIMURA T, TOZAWA K. Removal of arsenic from wastewater by addition of calcium hydroxide and stabilization of arsenic-bearing precipitate by calcinations [J]. Canadian Institute Mining, Metallurgy Petroleum, 1985, 878: 75−78.

[14] NAZARI A M, RADZINSKI R, GHAHREMAN A. Review of arsenic metallurgy: Treatment of arsenical minerals and the immobilization of arsenic [J]. Hydrometallurgy, 2017, 147: 258−281.

[15] ROBINS R G, HUANG J C Y, NISHIMURA T, KHOE G H. The adsorption of arsenate ion by ferric hydroxide [C]//Arsenic Metallurgy 1988. Warrendale, PA: TMS, 1988: 99−112.

[16] RIVEROS P A, DUTRIZAC J E, SPENCER P. Arsenic disposal practices in the metallurgical industry [J]. Canadian Metallurgical Quarterly, 2001, 40(4): 395−420.

[17] SWASH P M, MONHEMIUS A J. Synthesis, characterization and solubility testing of solids in the Ca−Fe−AsO_4 system [C]//Mining and the Environment 1988. Sudbury, PA: CANMET, 1995: 17−28.

[18] JAMBOR J L, DUTRIZAC J E. Occurrence and constitution of

natural and synthetic ferrihydrite, a widespread iron oxyhydroxide [J]. Chemical Reviews, 1998, 98(7): 2549−2586.

[19] FUJITA T, TAGUCHI R, ABUMIYA M, MATSUMOTO M, SHIBATA E, NAKAMURA T. Novel atmospheric scorodite synthesis by oxidation of ferrous sulfate solution. Part II: Effect of temperature and air [J]. Hydrometallurgy, 2008, 90(2−4): 85−91.

[20] DAIVID E C, FRANK C J, SCOTT F R. FRANK, R. Arsenic mobilization by the dissimilatory Fe(III)-reducing bacterium Shewanella alga BrY [J]. Environmental Science and Technology, 1999, 33(5): 723−729.

[21] DRAHOTA P, FILLIPPI M. Secondary arsenic minerals in the environment: A review [J]. Environment International, 2009, 35: 1243−1255.

[22] ZHU Y N, MERKEL B J. The dissolution and solubility of scorodite, $FeAsO_4·2H_2O$: Evaluation and simulation with PHREEQC2 [C]// Earth Enviromental Pollutant. Freiberg, Germany, 2001: 72−83.

[23] YUAN Zi-dan, ZHANG Dan-ni, WANG Shao-feng, XU Li-ying, WANG Kuan-ling, SONG Yu, XIAO Fan, JIA Yong-feng. Effect of hydroquinone-induced iron reduction on the stability of the scorodite and arsenic mobilization [J]. Hydrometallurgy, 2016, 164: 228−237.

[24] DUTRIZAC J E, JAMBOR J L. The synthesis of crystalline scorodite, $FeAsO_4·2H_2O$ [J]. Hydrometallurgy, 1988, 19(3): 377−384.

[25] LE BERRE J F, GAUVIN R, DEMOPOULOS G P. A study of the crystallization kinetics of scorodite via the transformation of poorly crystalline ferric arsenate in weakly acidic solution [J]. Colloids and Surfaces A: Physicochemical Engineering Aspects, 2008, 315(1): 117−129.

[26] DEMOPOULOS G P, DROPPERERT D J, VEERT G V. Precipitation of crystalline scorodite ($FeAsO·2H_2O$) from chloride solutions [J]. Hydrometallurgy, 1995, 38(3): 245−261.

[27] JIA Yong-feng, ZHANG Dan-ni, PAN Rong-rong, XU Li-ying, DEMOPOULOS G P. A novel two-step coprecipitation process using Fe(III) and Al(III) for the removal and immobilization of arsenate from acidic aqueous solution [J]. Water Research, 2012, 46: 500−508.

[28] FUJITA T, TAGUCHI R, ABUMIYA M, MATSUMOTO M, SHIBATA E, NAKAMURA T. Effects of zinc, copper and sodium ion on ferric arsenate precipitation in a novel atmospheric scorodite process [J]. Hydrometallurgy, 2008, 93: 30−38.

[29] KRAUSE E, ETTEL V A. Solubility and stability of scorodite, $FeAsO_4·2H_2O$: New date and further discussion [J]. American Minerals, 1988, 73: 850−854.

[30] KRAUSE E, ETTEL V A. Solubilities and stabilities of ferric arsenic compounds [J]. Hydrometallurgy, 1989, 22: 311−337.

[31] ADELMAN J G, ELOUATIK S, DEMOPOULOS G P. Investigation of sodium silicate-derived gels as encapsulants for hazardous materials: The case of scorodite [J]. Journal of Hazardous Materials, 2015, 292: 108−117.

[32] LAGNO F, ROCHA S D F, CHRYSSOULIS S, DEMOPOULOS G P. Scorodite encapsulation by controlled deposition of aluminum phosphate coatings [J]. Journal of Hazardous Materials, 2010, 181: 526−534.

[33] KARL L, GUO F, LEVENTE B, GOMEZ M A, DEMOPOULOS G P. Stabilization of iron arsenate solids by encapsulation with aluminum hydroxyl gels [J]. Journal of Chemical Technology Biotechnology, 2016, 91(2): 408−415.

[34] MIN Xiao-bo, LIAO Ying-ping, CHAI Li-yuan, YANG Zhi-hui, XIONG Shan, LIU Lin, LI Qing-zhu. Removal and stabilization of arsenic from anode slime by forming crystal scorodite [J]. Transactions of Nonferrous Metals Society of China, 2015, 25(4): 1298−1306.

[35] PETTINE M, CAMPANELLA L, MILLERO F J. Arsenite oxidation by H_2O_2 in aqueous solutions [J]. Geochimica et Cosmochimica Acta, 1999, 63(18): 2727−2735.

[36] CAETANO M L, CIMINELLI V S T, ROCHA S D F, SPITALE M C, CALDEIRA C L. Batch and continuous precipitation of scorodite from dilute industrial solutions [J]. Hydrometallurgy, 2009, 95: 44−52.

[37] CHEN T T, CABRIRI L J. Mineralogical overview of iron control in hydrometallurgical processing [C]//Iron Control in Hydrometallurgy. Chichester: Ellis Horwood, 1986: 19−55.

[38] JONES A M, GRIFFIN P J, WAITE T D. Ferrous iron oxidation by molecular oxygen under acidic conditions: The effect of citrate, EDTA and fulvic acid [J]. Geochimica et Cosmochimica Acta, 2015, 160: 117−131.

[39] LIANG Bo, HARTEL R W. Techniques for developing nucleation and growth kinetics from MSMPR data for sucrose crystallization in the presence of growth rate dispersion [J]. Journal of Crystal Growth, 1991, 108(1−2): 129−142.

[40] Hudson Institute of Mineralogy. Hudson Institute of Mineralogy, mindat.org database [EB/OL] [2017−10−03] https://www.mindat.org/min-3595.html.

[41] GOIA D V. Preparation and formation mechanisms of uniform metallic particles in homogeneous solutions [J]. Journal of Materials Chemistry, 2004, 14: 451−458.

[42] SINGHANIA S, WANG Q K, FILIPPOU D, DEMOPOULOS G P. Temperature and seeding effects on the precipitation of scorodite from sulfate solutions under atmospheric-pressure conditions [J]. Metallurgucal and Materials Transactions B, 2005, 36(3): 327−333.

[43] GOMEZ-GONZALEZ M A, BOLEA E, O'DAY P A, GARCIA-GUINEA J, GARRIDA F, LABORDA F. Combining single-particle inductively coupled plasma mass spectrometry and X-ray absorption spectroscopy to evaluate the release of colloidal arsenic from environmental samples [J]. Analytical Bioanalytical Chemistry, 2016, 408: 5125−5135.

[44] FRAU F, ROSSI A, ARDAU C, BIDDAU R, PELO D S, ATZEI D, LICHERI C, CANNAS C, CAPITANI G. Determination of arsenic speciation in complex environmental samples by the combined use of TEM and XPS [J]. Microchimica Acta, 2005, 151: 189−201.

[45] ZOUBOULIS A I, MOUSSAS P A, VASILAKOU E. Polyferric sulphate: Preparation, characterisation and application in coagulation experiments [J]. Journal of Hazardous Materials, 2008, 155: 459−468.

[46] FROST R L, LOPEZ A, SCHOLZ R, XI Y F, DA SILVEIRA A J, LIMA R M F. Characterization of the sulphate mineral amarantite−$Fe_2^{3+}(SO_4)O·7H_2O$ using infrared, Raman spectroscopy and thermogravimetry [J]. Spectrochimica Acta: Part A—Molecular and Biomolecular Spectroscopy, 2013, 114: 85−91.

[47] State Environmental Protection Administration and General Administration of Quality Supervision of the People's Republic of China, Standardization Administration of the People's Republic of China. Information and documentation—Rules for bibliographic references and citations to information resources: GB5080.3—2007 [S]. Beijing: Standards Press of China, 2007. (in Chinese)

[48] BLUTEAU M C, DEMOPOULOS G P. The incongruent dissolution of scorodite—Solubility, kinetics and mechanism [J]. Hydrometallurgy, 2007, 87: 163−177.

具有高浸出稳定性臭葱石的合成、原位包覆及表征

柯平超，刘志宏

中南大学 冶金与环境学院，长沙 410083

摘　要：为了提高臭葱石的稳定性，本文作者提出一种合成并原位包覆臭葱石的方法。在 Fe(II)−As(V)−H_2O 体系、90 ℃ 和 pH 1.5 的条件下持续通入氧气合成多面体状和山梅状臭葱石颗粒。当初始 Fe(II)/As(V)摩尔比超过 1:1 时，在合成过程中，一种含硫酸根的铁的氧化物或氢氧化物包覆层包覆在臭葱石颗粒表面。 为了检测这些合成样品的浸出稳定性，用TCLP毒性浸出方法对样品在pH 4.93进行60 h的浸出实验。此外，用多种不同pH 5.40~10.88浸出溶液对样品进行 30~40 d 的浸出实验。浸出结果表明，该包覆层能有效延缓臭葱石中砷的释放；TCLP 结果显示，其被包覆后砷的浸出浓度低至 0.12 mg/L，长周期浸出实验显示砷的浸出浓度低于 0.5 mg/L。

关键词：臭葱石；固砷；形核；原位包覆；稳定性

(Edited by Wei-ping CHEN)